Optimal Application of Damping to the Stanford Gravity Wave Experiment *

Frank A. McLoughlin†
013 Durand Building
(415)-723-1260

Daniel B. DeBra‡
028-B Durand Building
(415)-723-3388

Department of Mechanical Engineering
Stanford University, Stanford, California 94305

Abstract

This paper discusses the application of passive damping to the Stanford Gravity Wave Experiment [1,2,3]. The experiment's objectives and methodolgy are described, and mechanical design requirements are identified for this high order, cryogenically maintained, and very flexible structure. The need for damping in the structure is motivated, and the selection of passive magnetically induced eddy-current damping in lieu of active control as a baseline is discussed. A design procedure which attempts to optimally allocate viscous damping elements in linear discrete structures is presented. Damper sizing and design considerations aimed at providing a stiffness–damping structural impedance match are also discussed.

1 Introduction

1.1 Experiment Description

The Stanford Gravity Wave Experiment apparatus shown in Figure 1 is aimed at sensing the infinitesimal momentum and energy carried by the gravity waves predicted by Einstein's general theory of relativity, and which result from the motion of objects in space. The energy content of gravity waves is extremely small. Only gravity waves associated with galactic phenomena such as stellar collapses can hoped to be distinguished at this time. The experiment consists of sensing gravity waves by making state-of-the-art measurements of their dynamical interaction with the first longitudinal vibration mode of a 4800 kg aluminum bar (see Figure 2). The bar consequently acts as a gravity wave *antenna*, and is designed to have its first longitudinal vibration mode at about 850 Hz. Sensing of

*Supported by NSF under contract PHY85–05755 and by TRW Space and Technology Group
†Graduate Research Assistant
‡Professor of Aeronautics and Astronautics and Mechanical Engineering

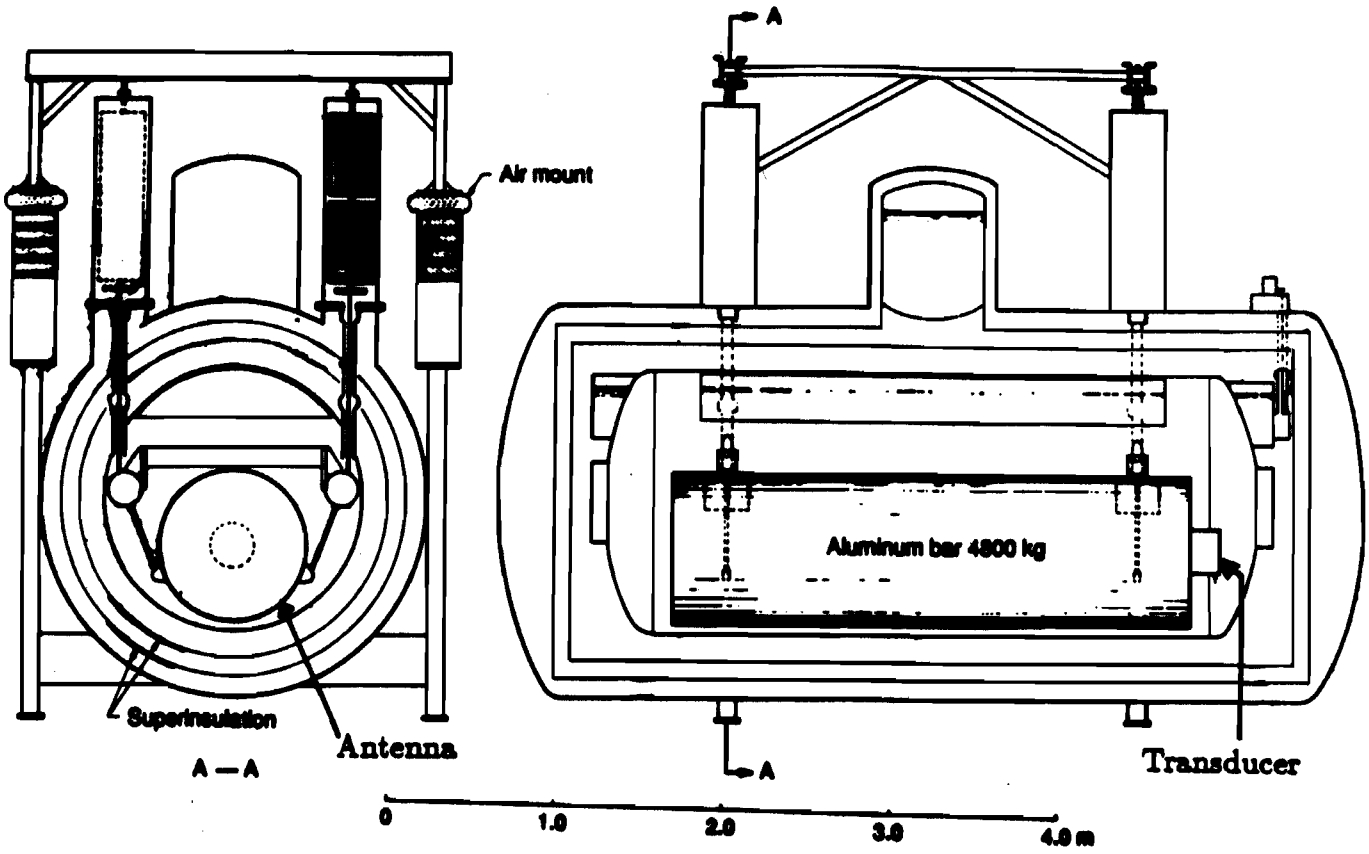

Figure 1: Schematic diagram of the 4800 kg cryogenic gravity wave detector at Stanford University

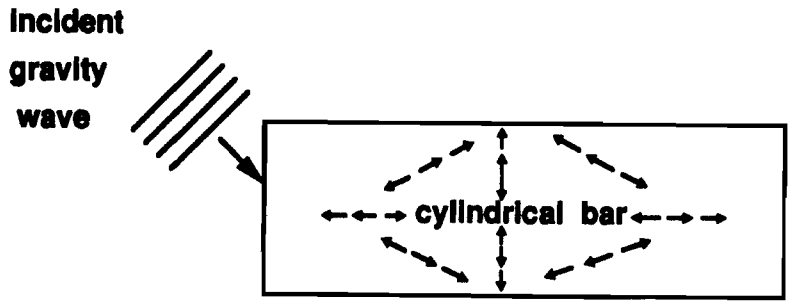

Figure 2: Incident gravity waves induce strain in cylindrical bar

the longitudinal strain in the bar is performed with a superconducting variable inductance resonant transducer and SQUID amplifier [2,3].

Because of the weakness of these signals, a great deal of effort is spent minimizing disturbances to the antenna. To reduce Brownian noise disturbances [4] sufficiently for the level of sensing required, the antenna is held at a temperature of 4 K. The antenna is also isolated from cultural and seismic ground disturbances in the laboratory by 250 dB at the frequency of its longitudinal resonance. Furthermore, the antenna is maintained in a near vacuum to minimize the possibility of acoustic disturbances propagating through air to the antenna. To amplify the dynamical interaction of interest, and to consequently make the sensing possible, the antenna is made of a high mechanical quality factor, Q, material [2]. For the existing system, the antenna is made of Aluminum and has a Q of $\sim 4 \times 10^6$ ($Q = 1/2\zeta$, ζ=damping ratio) at 4 K in the mode of interest.

Isolation of the antenna from external disturbances is provided by an isolation system consisting of four isolation stacks each with ten spring–mass pairs for high frequency isolation, and an air bag for low frequency isolation (see Figure 1). 250 dB of mechanical isolation in 6 degrees of freedom over a 200 Hz bandwidth centered at 850 Hz is provided by this system. The isolation system is also external to, and thermally insulated from the cryogenic region housing the antenna.

The next generation gravity wave detector at Stanford University[1] is currently being designed (see Figure 3). A comparison between the characterstics of the existing system and the goals of the next generation system is provided in Table 1. The goal of the new system is a 1 to 2 order of magnitude increase in measurement sensitivity. To this end, the new system will maintain the antenna at 40 mK to reduce Brownian noise and to further increase the signal-to-noise ratio. In order to uncouple the thermal and isolation design problems, and to minimize interaction with internally generated and difficult to identify noise sources, the present strategy is to enclose the vibration isolation system in the low temperature region.

The springs and masses for the next generation isolation system are currently being designed. The objective is to design spring elements which will, when stacked together, be compliant enough to provide the isolation required at the antenna longitudinal resonance frequency. Concurrently, the springs must statically support the weight of the antenna with minimal stress in the spring material. The motivation for minimizing stress levels in the springs is discussed in section 1.2. The goal is to have the maximum static stress in the springs be less than 10% of the 0.2% yield stress of the material.

In addition to stiffness properties, another issue underlying material selection is the way in which the system's components can be interfaced. As is discussed in section 1.2, the system cannot tolerate nonlinear disturbance energy resulting from *sloppy* joints. All components of the isolation system must be connected with welds or brazes which have as close to a monolithic interface structure as possible. The materials currently under consideration for spring fabrication are beryllium–copper and aluminum (e. g. Al 7075).

Note that the isolation must be provided in 6 DOF (degrees of freedom). The approach taken is to design the springs and masses so that the same resonant frequencies are obtained

[1]Sponsored by NSF. Peter Michelson is principal investigator.

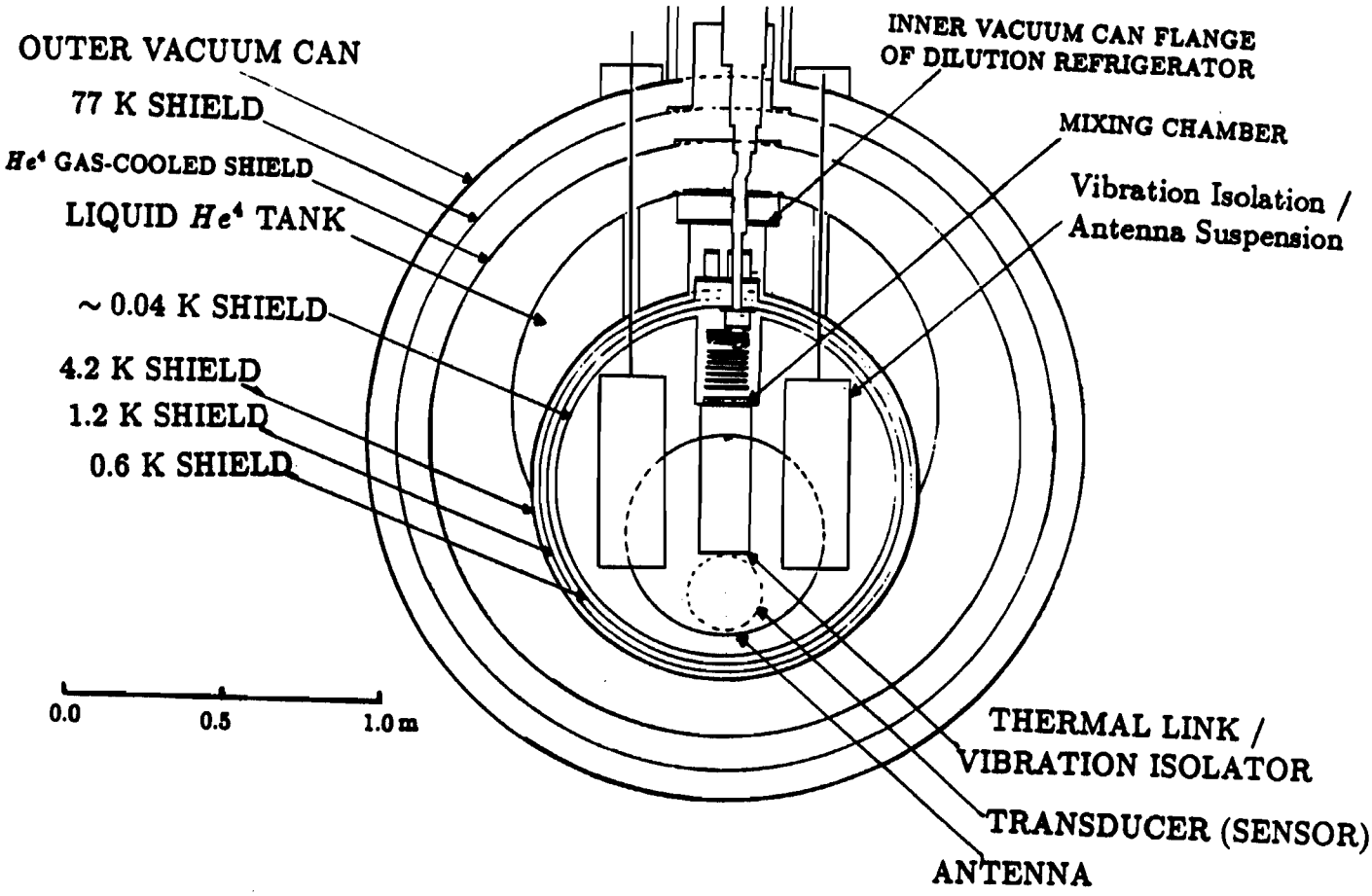

Figure 3: Next generation ultra–low temperature gravity wave detector cryostat

parameter	purpose	existing system	next generation
isolation	- isolate antenna from ground (seismic & cultural) - must be as purely linear as possible in dynamic range	250 dB over 200 Hz BW centered at antenna resonance	300 dB over 200 Hz BW about antenna resonance
temperature	- minimize brownian noise in antenna - allow operation of superconducting sensor	4 K	40 mK
pressure	- minimize disturbances on antenna due to air (e.g. acoustic)	~ vacuum	~ vacuum
antenna longitudinal damping	- High Q material reduces brownian motion noise	$Q \approx 4 \times 10^6$	$Q > 10^7$ ($\zeta < 5\,(10^{-8})$)
sensing	- inductive superconducting resonant transducer and SQUID amplifier	strain ($\Delta l / l$) $\approx 10^{-18}$	strain ($\Delta l / l$) $\approx 10^{-20}$

Table 1: Gravity Wave Experiment characteristics

in each DOF. To this end, consider basis unit vectors x, y, and z of a cartesian coordiante frame fixed in the laboratory. Let k_x, k_y, and k_z be linear translational stiffnesses and let k_{θ_x}, k_{θ_y}, and k_{θ_z} be linear rotational stiffnesses of the springs for the designated axes. Similarly, let each mass element have mass m and central moments of inertia I_x, I_y, and I_z for axes x, y, and z, respectively. Matching resonant frequencies requires that for each spring–mass pair:

$$\omega_r = \sqrt{\frac{k_i}{m}} = \sqrt{\frac{k_{\theta i}}{I_i}} \ , \quad (i = x, y, \text{ and } z). \tag{1}$$

The current spring configuration is shown in the hashed portion of Figure 4(a). The springs have a *clover-leaf* like configuration. Each lobe of the *clover-leaf* springs acts between two mass elements of the isolation stack. The concept for interfacing the spring and mass elements is shown in Figure 4(b). The mass elements are shown as H–shaped bodies which are intended to be approximately rigid.

1.2 Damping Issues

The previous section described objectives and system level issues for the existing and next generation gravity wave detectors at Stanford. This section motivates the need for damping in the isolation system of the next generation experiment. There are two issues. First is the baseline decision to place the isolation system in the coldest temperature region, and

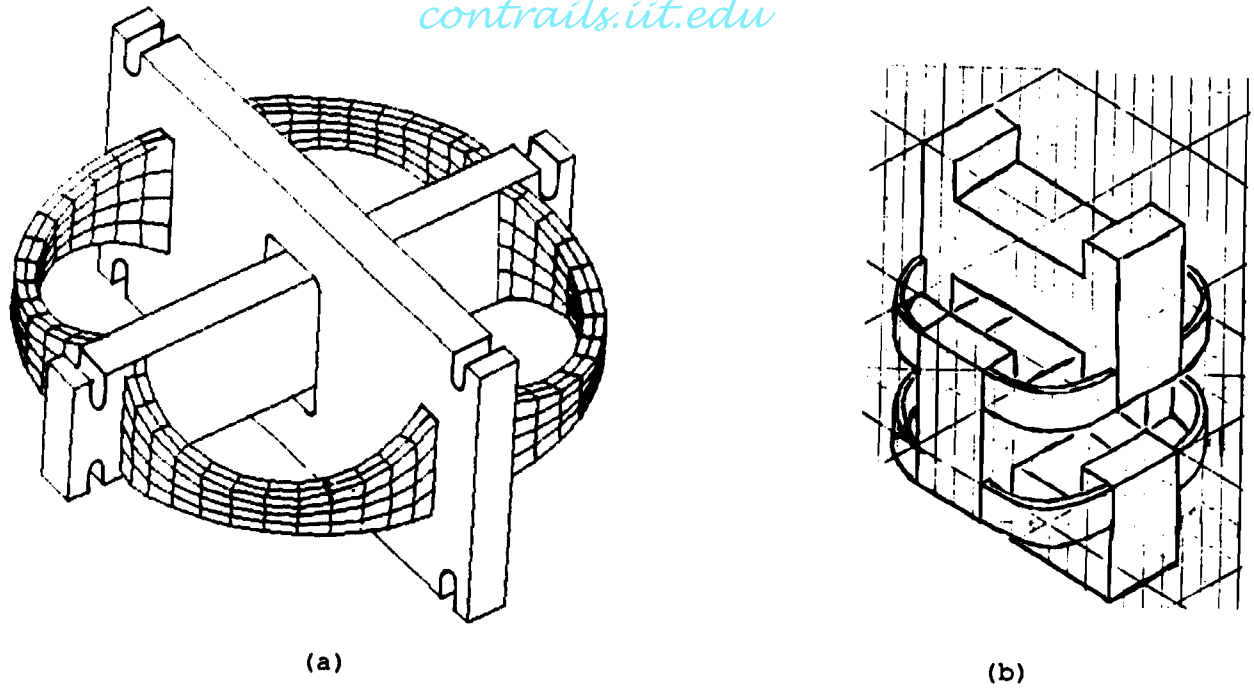

Figure 4: Isolation system concept: (a) isolation spring element, and (b) spring–mass interfacing concept.

second is increased concern associated with the sensitivity to nonlinear *creaking* in the system.

At 40 mK the isolation system itself will have mechanical Q's on the order of 10^7 or higher in all of its vibrational modes (see Figure 5) [4,5]. The resulting amplification of the spectral content of the disturbances at the resonant frequencies ($\sim 70 - 250$ Hz) of the isolation system poses a key problem. These greatly amplified inputs may cause the system to deviate from purely linear behavior. The effect is conversion of the narrow band input disturbance into a broadband disturbance. Sufficient energy at the 850 Hz antenna mode resulting from the broadband disturbance may corrupt the measurements. Although physical mechanisms for this type of nonlinear behavior have not been clearly identified for this system, hypotheses have been formulated. Among these are the hypotheses that the large amplification of low frequency disturbances causes nonlinear *creaking* at stress concentration areas of joints throughout the system. These concentrations of stress can result in local hysteretic deformations of the material which can propagate as broadband acoustic energy [2,6].

Design candidates for mitigating this problem include actively and/or passively damping the isolation system. The goal is to remove mechanical energy from the system which results from low frequency disturbance amplification. The effect of damping is to reduce the steep but narrow, and consequently relatively low energy, resonant peaks in the isolation's frequency response. In addition to reducing these peaks, added damping will reduce the RMS (root mean square) dynamic stresses in the isolation springs. This in turn will reduce the probability of localized hysteretic deformations which result in broadband disturbances.

In regard to implementing damping for this system, there are a few interesting constraints which must be considered. First, the damping must be realizable at ultra–low

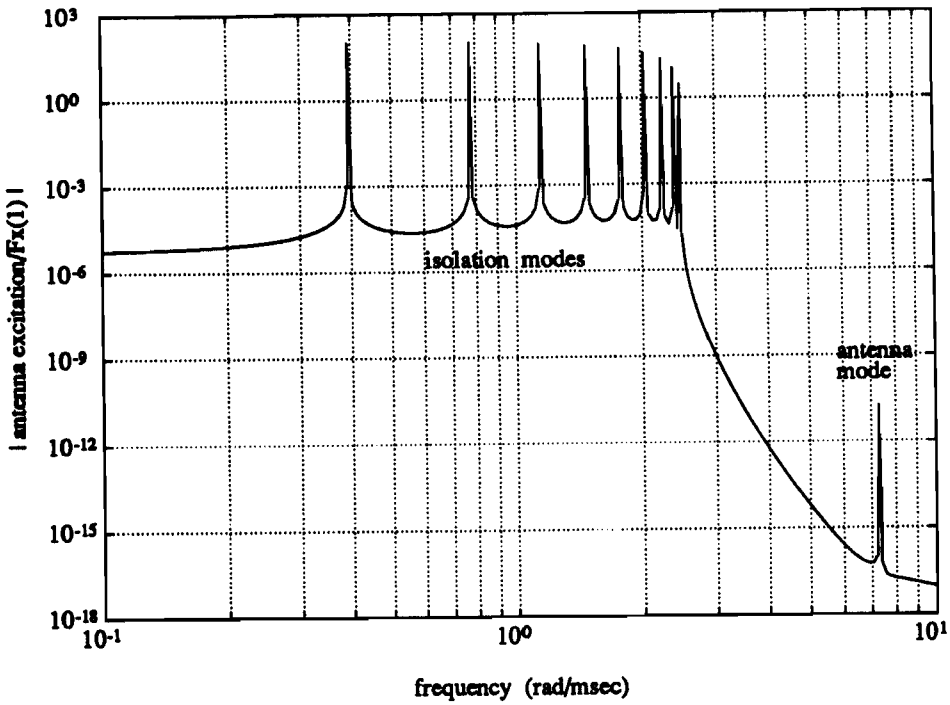

Figure 5: Undamped frequency response ($Q = (10)^7$) from input at top of isolation stack in x-direction to antenna excitation

temperatures. Potential energy dissipation candidates at this point include electronic absorption of ultra-sounds, low temperature relaxation of dislocations, magnetic hysteresis, dry friction, or magnetically induced eddy-current damping [7]. Futhermore, the damping is required to be predictable/repeatable, and it is required that the damping mechanism not have substantial energy content at the antenna longitudinal resonance frequency. Consequently dry friction, for example, is inappropriate because of the broadband spectral content of this nonlinear phenomenon. Another interesting design issue which is discussed in section 6, is matching the impedance between the dampers and the stiffness elements.

The baseline approach is to use passive eddy-current damping. The negligible impact of the low temperature environment upon permanent magnets make this phenomenon realizable at low temperatures. Furthermore, eddy-current damping devices can be designed to provide nearly purely viscous damping, and can be made free of ***sloppy*** nonlinear joints. Finally, by using a superconducting wire, the energy absorbed by the eddy-current damper can be dissipated in an external resistor in a warmer region of the dewar. The concern regarding remotely dissipating energy, however, is that the damper then has the Brownian motion noise of the warmer region where the energy is being dumped.

Among the key design parameters are the placement and sizing of the dampers. Summarized below are design considerations which guided the definition of these parameters.

- The added damping should minimize the RMS dynamic strain in the isolation system's modes.
- The added damping should not compromise the isolation provided to the antenna.

- The 1st longitudinal resonance mode of the antenna is intentionally very lightly damped for measurement purposes. The added damping should damp the isolation system modes without damping this antenna mode.

- Energy dissipated as heat cannot be arbitrarily dissipated in the system. Because of the severe refrigeration requirements at the lowest temperature region, only about 10 μW of power dissipation as heat can be tolerated in this region. In the warmer insulation shells, such as the 0.6 K shell (see Figure 3), as much as 1 mW of heat can be tolerated.

The sections that follow discuss how these considerations were used to establish baseline damping allocation requirements for the Gravity Wave Experiment system.

2 Damping Allocation Design Procedure

This section discusses a design procedure being developed which is aimed at aiding a structural designer to identify the degree to which damping can be of value, and to identify locations on a structure which are in some sense optimal for the inclusion of damping. The procedure also identifies levels of viscous damping which are also optimal in some sense. Furthermore, the procedure is automated by software written in PRO–MATLAB [8] and FORTRAN 77.

The motivation for the development of such a tool is to include damping as a parameter in the design of controlled structures. The potential payoffs are numerous. Recent studies (e. g. Passive and Active Control of Space Structures (PACOSS)) have demonstrated that passively included damping elements can reduce the number of control actuators and total control energy required in some large flexible structure control problems. Futhermore, when actively controlling a structure, a higher closed–loop bandwidth can frequently be achieved by adding damping to an otherwise lightly damped structure.

The task of identifying an optimal allocation of damping in a structure is complicated by many design issues. Certainly cost, complexity, repeatability, geometry, and environmental conditions are just a few of the many typical design considerations. These considerations can have quite varied characters, are often difficult to quantify, and can be difficult to compare on an equal footing for trade-off purposes. Furthermore, the damping which can be incorporated into a structure may be distributed or discrete, may have a wide range of thermal or frequency dependencies [7], and may vary nonlinearly with amplitude or velocity.

The design procedure described here focuses on outputs derivable from the response of a linear structure to external inputs. The goals are to determine locations on a structure where damping elements will have their greatest influence on specific outputs, and to identify the level of influence at these outputs. Typical outputs may include the response of a radio frequency antenna mounted on a spacecraft or the control energy required by actuators on a structure.

A key underlying idea in the damping allocation optimization scheme used here is that damper placement should be tailored to a system's specific input and output characteris-

tics. Consequently, specific information regarding a system's input locations, directions, and spectral content, as well as outputs of interest, must be available. The outputs must be derivable from a linear combination of the states (i.e. positions and velocities) of the system. A cost function computed as a weighted norm of the RMS or 1σ values of the states of a discrete linear system model is used to determine an optimal damping allocation. This condition on the types of outputs allowable is not as restrictive as it may seem. As will be discussed in section 4, outputs which have been used include the resonant excitation of a large flexible bar (the Stanford Gravity Wave antenna), the average power dissipated as heat in dampers placed on a structure, and the dynamic strain induced in elements throughout a structure. Furthermore, should the peak rather than RMS value of an output be regarded as the appropriate quantity for optimization, then a reasonable approximation to the peak can be obtained by considering the 3σ or 4σ value of the output.

An important feature in this damping allocation procedure is the specific emphasis on the sensitivity of damper placement to specific input and output characteristics. Methods for damping allocation which are based solely on modal strain energy considerations, for example, and which attempt to identify energy concentration areas and consequently attempt to minimize the global energy in a system , may result in effort expended to remove energy that does not seriously impact outputs of interest. Futhermore, there is a possibility of a mode of vibration with relatively little energy, but for which an important output is seriously impacted. An example may be the vibration of a small antenna on a massive spacecraft. Another consideration is the possibility that inputs to a structure may have points of application, directions, or spectral content which do not significantly excite the vibration modes for which outputs of interest have large mode shape values.

2.1 Assumptions

Several assumptions underlie the design procedure developed. The procedure requires the existence of a nominal structural model. The dynamics of the structure must be describable by a linear, constant coefficient, matrix equation of the form:

$$[M]\{\ddot{x}\} + [C]\{\dot{x}\} + [K]\{x\} = \{f(t)\} \tag{2}$$

where [M], [C], and [K] are the time–invariant mass, viscous damping, and stiffness matrices, respectively, of the structure associated with the n generalized coordinates comprising the vector $\{x\}$. {f(t)} is a time dependent vector of input forces. The mass and stiffness matrices, [M] and [K], are assumed to be real and symmetric, and the stiffness matrix is assumed positive definite. The viscous damping matrix must be real, and need not be proportional damping (i.e. a linear combination of the mass and stiffness matrices). These assumptions consequently require a discrete linear structural model, such as is available from finite element software packages. In the case of a finite element model of the structure, the generalized coordinates are the node displacements in all active degrees of freedom.

The nominal structure is assumed asymptotically stable. Consequently some positive viscous damping must be modeled in each mode of the nominal structure, though the damping in each mode may be arbitrarily small.

There can be an arbitrary number of temporally uncorrelated external forces acting on the structure. These forces can be applied at arbitrary nodes and in any direction. The input forces must be capable of being modeled as filtered zero-mean, gaussian, ergodic, white noise. The coloring filters, which define the spectral content of the input forces, must be strictly proper continuous filters with no poles at the origin.

Damping added to the nominal structural model is assumed to be in the form of purely viscous discrete damping elements. Each element is attached to the structure at two distinct nodes. Furthermore, each damping element may provide damping in as many as six degrees of freedom, with an arbitrary viscous damping constant in each degree of freedom.

2.2 Candidate Damper Locations

The design procedure consists of two steps: a more synthetic step discussed in this section, and an optimization step discussed in the next section. The synthetic step is aimed at identifying *good* candidate locations for placing dampers in a structure. In the optimization step, the candidate locations are compared by determining the impact upon outputs of interest of placing dampers at these locations.

Several approaches can be taken to identify good locations for dampers. The approach taken here is motivated by an attempt to identify which locations on a structure have the greatest *influence* upon the outputs of interest. The result is the development of easily computed influence coefficients. The coefficients consider the location and spectral content of external inputs as well as the system outputs.

Consider the modal coordinates for a system described by equation (2). The modal coordinates $\{\eta\}$ are related to the physical coordinates $\{x\}$ by:

$$\{x\} = [U]\{\eta\} \tag{3}$$

where [U] is the system's real $n \times n$ matrix of eigenvectors (mode shapes) normalized according to:

$$[U]^T[M][U] = [I_n], \tag{4}$$

where $[I_n]$ is the $n \times n$ identity matrix. Using (3) and (4), the system's dynamical equations can be expressed in modal coordinates as:

$$\{\ddot{\eta}\} + [2\zeta\Omega]\{\dot{\eta}\} + [\Omega^2]\{\eta\} = [U]^T\{f(t)\} \tag{5}$$

where $[2\zeta\Omega]$ and $[\Omega^2]$ are real diagonal matrices of modal damping and natural frequencies squared, respectively. Note, it has been assumed that the nominal system's inherent damping matrix, [C], has sufficiently small damping to be at least approximately uncoupled by a coordinate transformation using [U]. Taking the Laplace transform of (5) ignoring initial conditions yields:

$$\eta(s) = ([I_n]s^2 + [2\zeta\Omega]s + [\Omega^2])^{-1}[U]^T\{F(s)\} \tag{6}$$

so that using (3):

$$x_j(s) = \sum_{i=1}^{n} \frac{u_{j,i}}{s^2 + 2\zeta_i\omega_i s + \omega_i^2}\{u_i\}^T F(s) \tag{7}$$

where x_j is the j^{th} element of $\{x\}$, $\{u_i\}$ is the i^{th} mode shape (column of [U]), $u_{j,i}$ is the j^{th} element of $\{u_i\}$, ζ_i is the damping ratio of mode i, and ω_i is the natural frequency of mode i $(i = 1, \ldots, n)$.

Now consider the effect of introducing to the nominal system, a discrete viscous damping element acting between generalized coordinates x_a and x_b $(1 \leq a, b \leq n)$. Assuming for the moment that this damper is massless, the dynamical effect on the system is identical to the effect of adding equal magnitude but oppositely directed forces at x_a and x_b which are proportional to the relative velocity between these coordinates. These damping forces can be considered by adding a force vector in equation (2) with forcing terms in the a^{th} and b^{th} elements, that is:

$$f_{damp}^T = \left[\overbrace{0 \ \ldots \ 0 \ c(\dot{x}_b - \dot{x}_a)}^{a} \ 0 \ \ldots \ 0 \ \underbrace{-c(\dot{x}_b - \dot{x}_a)}_{b} \ 0 \ \ldots \ 0 \right]. \tag{8}$$

Considering only the contribution of these damping forces to $x_j(s)$, we can write

$$x_j(s) = \sum_{i=1}^{n} \frac{u_{j,i}(u_{a,i} - u_{b,i})c}{s^2 + 2\zeta_i\omega_i s + \omega_i^2} s(x_b(s) - x_a(s)). \tag{9}$$

In fact, these damping forces result when relative motion between coordinates x_a and x_b is induced by external forces. With this in mind, and noting that $x_a(s)$ and $x_b(s)$ in equation (9) can be expressed in the same form as $x_j(s)$ in equation (7):

$$x_j(s) = \sum_{i=1}^{n} \frac{u_{j,i}(u_{a,i} - u_{b,i})c}{s^2 + 2\zeta_i\omega_i s + \omega_i^2} \left[\sum_{k=1}^{n} \frac{(u_{b,k} - u_{a,k})s}{s^2 + 2\zeta_k\omega_k s + \omega_k^2} \{u_k\}^T \right] F(s). \tag{10}$$

Now consider the case in which the external force consists only of a force applied at coordinate m, and also only consider the contribution to $x_j(s)$ from mode r ($i = r$ in equation (10)) and express this as $(x_{j,m})_r$:

$$(x_{j,m})_r(s) = \frac{u_{j,r}(u_{a,r} - u_{b,r})c}{s^2 + 2\zeta_r\omega_r s + \omega_r^2} \left[\sum_{k=1}^{n} \frac{(u_{b,k} - u_{a,k})s}{s^2 + 2\zeta_k\omega_k s + \omega_k^2} u_{m,k} \right] F_m(s). \tag{11}$$

Recalling that the objective is to identify some measure of *influence* from an input to an output with discrete viscous damping acting between two arbitrary coordinates, it can be seen that equation (11) expresses this influence, with m as the input coordinate, j as the output coordinate, and a and b as the coordinates between which the damper acts.

Now let s vary along the $J\omega$–axis ($J = \sqrt{-1}$), emphasizing an interest in the dependence of this influence upon the spectral content of the input, to obtain:

$$(x_{j,m})_r(J\omega) = \frac{u_{j,r}(u_{a,r} - u_{b,r})c}{\omega_r^2 - \omega^2 + J * 2\zeta_r\omega_r\omega} \left[\sum_{k=1}^{n} \frac{(u_{b,k} - u_{a,k})J\omega}{\omega_k^2 - \omega^2 + J * 2\zeta_k\omega_k\omega} u_{m,k} \right] F_m(J\omega). \tag{12}$$

Evaluating at $\omega = \omega_r$, since it is the contribution of mode r under consideration, the following measure of the gain or influence at mode r associated with an input at coordiante

m, an output at coordinate j, and a viscous damper acting between coordinates a and b is obtained:

$$\left| \frac{u_{j,r}(u_{a,r} - u_{b,r})c}{2\zeta_r \omega_r^2} \left[\sum_{k=1}^{n} \frac{(u_{b,k} - u_{a,k}) J\omega_r}{\omega_k^2 - \omega_r^2 + J * 2\zeta_k \omega_k \omega_r} u_{m,k} \right] \right| |F_m(J\omega_r)|. \tag{13}$$

Furthermore, for outputs of interest which are linear combinations of system states, such as:

$$\{y\} = [C]\{x\}, \text{ so that } y_j = \sum_{i=1}^{n} C(j,i)x(i) \tag{14}$$

where [C] is a real constant *outputs* $\times$ n matrix, then the influence coefficient for output y_j is obtained by replacing $u_{j,r}$ in equation (13) with $\sum_{i=1}^{n} C(j,i)u_{i,r}$.

A PRO–MATLAB function has been written to automate the computation and sorting of these influence coefficients. By easily specifying input locations, the spectral content at each input location, outputs, and damping coordinate pairs, this function aids a designer to generate a first cut at good candidate damper locations. Futhermore, by ranking the influence coefficients by mode, one can identify which modes are most significant for the inputs, outputs, and damper locations considered. Application of this procedure to the Stanford Gravity Wave Experiment is discussed in section 3.

2.3 Optimization Analysis

Section 2.2 discussed a procedure to generate a collection of *good* candidate damper locations in a structure. This section discusses an analysis tool developed to evaluate the impact of incorporating viscous damping elements in a controlled structure. The objective of this tool, which is fully automated in PRO–MATLAB software [8], is to identify which of a collection of candidate damper placement scenarios in a structure is optimal for a particular application, and furthermore what level of damping is appropriate. The hope is that damping will be allocated in an efficient way to adequately damp all important modes. Each damper allocation case considered can include an arbitrary number of arbitrarily distributed and directed damping elements, each with arbitrary viscous damping constant. Furthermore, the procedure will include the impact upon a nominal structure of damping elements with arbitrary mass and stiffness properties. Typical of candidate damper locations to consider are those generated by the algorithm of section 2.2.

Several inputs are required for this analysis. A nominal discrete linear (finite element) model must exist for the structure under consideration. The model must consist of $n \times n$ mass, stiffness, and viscous damping matrices, where n is the number of active structural degrees of freedom. The location, direction, and spectral content of all inputs must be known. Finally, a collection of outputs of interest must be identified.

This section begins by constructing a state-space realization for a general system considered. This realization demonstrates the ability to address systems which include structural dynamics states; sensor, actuator, and estimator states as needed; and coloring filter states to model the spectral character of external inputs. The topology for the optimization, as well as the structure of the performance index used is then discussed. A procedure to sub-optimize over damping constant values for each case is also discussed.

A state space model for the nominal structure, or plant, is modeled using plant coordinates, $\{x_p\}$, as:

$$\{\dot{x}_p\} = [A_p]\{x_p\} + [B_{px}]\{f_x(t)\} + [B_{pc}]\{f_c(t)\} \tag{15}$$

where,

$$\{x_p\} \triangleq \left\{ \begin{array}{c} x \\ \dot{x} \end{array} \right\}, \; [A_p] \triangleq \left[\begin{array}{cc} 0 & I_n \\ -M^{-1}K & -M^{-1}C \end{array} \right], \tag{16}$$

$$[B_{px}] \triangleq \left[\begin{array}{c} 0 \\ -M^{-1}B_x \end{array} \right], \; [B_{pc}] \triangleq \left[\begin{array}{c} 0 \\ -M^{-1}B_c \end{array} \right]. \tag{17}$$

[M], [C], [K], and $\{x\}$ are as defined in equation (2), and I_n is the $n \times n$ identity matrix. $\{f_x(t)\}$ is a vector of m_x external inputs and $\{f_c(t)\}$ is a vector of m_c control inputs. $[B_x]$ and $[B_c]$ are input distribution matrices for external inputs and control inputs, respectively. Note that for numerical stability, care must be taken to select appropriate units for [M], [C], and [K] so that $[A_p]$ is well conditioned.

Now consider the inclusion of actuator dynamics to the nominal plant. Let $\{f_c(t)\}$ be the vector of controls actually input to the plant, and $\{u_a(t)\}$ be the vector of actuation commands. Furthermore, let a state space realization from the i^{th} actuator input, $f_{c,i}$, to the i^{th} actuator command, $u_{a,i}$, be given by:

$$\{\dot{x}_{a,i}\} = [\alpha_{a,i}]\{x_{a,i}\} + \{\beta_{a,i}\}u_{a,i} \tag{18}$$

$$f_{c,i} = [\gamma_{a,i}]\{x_{a,i}\} + \delta_{a,i}u_{a,i} \tag{19}$$

The combined plant–actuator system can then be realized as:

$$\{\dot{x}_{pa}\} = [A_{pa}]\{x_{pa}\} + [B_{pa}]\{u_a\} + [B_{px}]\{f_x\} \tag{20}$$

where,

$$\{x_{pa}\} \triangleq \left\{ \begin{array}{c} x_p \\ x_a \end{array} \right\}, \; [A_{pa}] \triangleq \left[\begin{array}{cc} A_p & B_{pc}\Gamma_a \\ 0 & A_a \end{array} \right], \; [B_{pa}] \triangleq \left[\begin{array}{c} B_{pc}\Delta_a \\ B_a \end{array} \right], \tag{21}$$

$$[A_a] \triangleq diag[\, \alpha_{a,1} \; \alpha_{a,2} \; \cdots \; \alpha_{a,m_c} \,], \;\; [B_a] \triangleq diag[\, \beta_{a,1} \; \beta_{a,2} \; \cdots \; \beta_{a,m_c} \,], \tag{22}$$

$$[\Gamma_a] \triangleq diag[\, \gamma_{a,1} \; \gamma_{a,2} \; \cdots \; \gamma_{a,m_c} \,], \;\; [\Delta_a] \triangleq diag[\, \delta_{a,1} \; \delta_{a,2} \; \cdots \; \delta_{a,m_c} \,]. \tag{23}$$

The notation $diag[\cdots]$ refers to a block diagonal matrix with the arguments on the diagonal. $[A_a]$, for example, is a block diagonal matrix with the blocks $\alpha_{a,i}$ $(i = 1, \ldots, m_c)$ on the diagonal.

Now consider the inclusion of sensor dynamics to the nominal plant–actuator system. Let $[C_m]$ be a real constant measurement matrix such that an m_s-vector of ideal measurements, $\{y_{ideal}\}$, is given by:

$$\{y_{ideal}\} = [C_m]\{x_{pa}\} \tag{24}$$

To accommodate sensor dynamics, let a state space realization from the i^{th} element of $\{y_{ideal}\}$ to the i^{th} element of the actual measurement vector, $\{y\}$, be given by:

$$\{\dot{x}_{s,i}\} = [\alpha_{s,i}]\{x_{s,i}\} + \{\beta_{s,i}\}y_{ideal,i} \tag{25}$$

$$y_i = [\gamma_{s,i}]\{x_{s,i}\} + \delta_{s,i} y_{ideal,i} \tag{26}$$

The combined plant–actuator–sensor system can then be realized as:

$$\{\dot{x}_{pas}\} = [A_{pas}]\{x_{pas}\} + [B_{pa}]\{u_a\} + [B_{px}]\{f_x\} \tag{27}$$

where,

$$\{x_{pas}\} \triangleq \begin{Bmatrix} x_{pa} \\ x_s \end{Bmatrix}, \quad [A_{pas}] \triangleq \begin{bmatrix} A_{pa} & 0 \\ B_s C_m & A_s \end{bmatrix}, \tag{28}$$

$$[A_s] \triangleq diag[\, \alpha_{s,1}\ \alpha_{s,2}\ \cdots\ \alpha_{s,m_s}\,], \quad [B_s] \triangleq diag[\, \beta_{s,1}\ \beta_{s,2}\ \cdots\ \beta_{s,m_s}\,], \tag{29}$$

and note that {y} is given by:

$$\{y\} = [C_s]\{x_{pas}\}, \quad \text{where} \quad [C_s] \triangleq \begin{bmatrix} \Delta_s C_m & \Gamma_s \end{bmatrix} \tag{30}$$

where,

$$[\Gamma_s] \triangleq diag[\, \gamma_{s,1}\ \gamma_{s,2}\ \cdots\ \gamma_{s,m_s}\,], \quad [\Delta_s] \triangleq diag[\, \delta_{s,1}\ \delta_{s,2}\ \cdots\ \delta_{s,m_s}\,]. \tag{31}$$

Now consider designing a control system for the structure being considered. To this end, assume that the control law generated is in the form of feedback of estimated plant, actuator, and sensor states. Simpler control laws, such as feedback of sensor outputs alone with no estimation, are a subset of this more general construction. Actuator commands are then given by:

$$\{u_a\} = -[K]\{\hat{x}_{pas}\} \tag{32}$$

where [K] is constant control gain matrix and $\{\hat{x}_{pas}\}$ is a vector of estimated plant, actuator, and sensor states. [K] may, for example, be the gains resulting from a solution of the linear quadratic regulator (LQR) control optimization problem [9]. The estimator state equation is assumed to be of the following form:

$$\{\dot{\hat{x}}_{pas}\} = [A_{pas}]\{\hat{x}_{pas}\} + [B_{pa}]\{u_a\} + [L]\,[\{y\} - [C_s]\{\hat{x}_{pas}\}]\,. \tag{33}$$

[L] is a constant estimator gain matrix, and may, for example, be the steady state Kalman-Bucy filter gains associated with the linear quadratic estimator (LQE) optimization problem [9].

By combining equations (27), (32), and (33), the entire system can be realized as:

$$\{\dot{x}_{pase}\} = [A_{pase}]\{x_{pase}\} + [B_{px}]\{f_x\} \tag{34}$$

where,

$$\{x_{pase}\} \triangleq \begin{Bmatrix} x_{pas} \\ \hat{x}_{pas} \end{Bmatrix}, \quad [A_{pase}] \triangleq \begin{bmatrix} A_{pas} & -B_{pa}K \\ LC_s & A_{pas} - B_{pa}K - LC_s \end{bmatrix}. \tag{35}$$

Finally, consider the inclusion of continuous filter states used to shape the spectral content of the m_x–vector of external inputs, $\{f_x\}$. The external forces can be the result of a directly applied force, or the result of external *ground* motion acting through linear translational or rotational springs and/or viscous dampers. It is assumed that the MSSD (mean square spectral density) also referred to as the PSD (power spectral density) of

either the applied force or ground motion is known, and can be adequately modeled as continuously filtered white noise. The Laplace transform of the coloring filters is assumed to have no purely imaginary poles. The i^{th} external input can be written as:

$$f_{x,i} = k_{x,i}\phi_{x,i} + c_{x,i}\dot{\phi}_{x,i} \quad (i = 1, \ldots, m_x) \tag{36}$$

where $\phi_{x,i}$ is the i^{th} filtered input. Let a state space realization from an external input with a white PSD, $\omega_{x,i}$, through the i^{th} shaping filter to $\phi_{x,i}$ be written as:

$$\{\dot{x}_{x,i}\} = [\alpha_{x,i}]\{x_{x,i}\} + \{\beta_{x,i}\}\omega_{x,i} \tag{37}$$

$$\phi_{x,i} = [\gamma_{x,i}]\{x_{x,i}\} + \delta_{x,i}\omega_{x,i} \tag{38}$$

Now assume that the transfer function of these filters in the Laplace domain is strictly proper so that $\delta_{x,i} = 0$ $(i = 1, \ldots, m_x)$. Then by substituting equations (37) and (38) into equation (36):

$$f_{x,i} = [a_{kc,i}]\{x_{x,i}\} + b_{kc,i}\omega_{x,i} \tag{39}$$

where,

$$[a_{kc,i}] \triangleq k_{x,i}[\gamma_{x,i}] + c_{x,i}[\gamma_{x,i}][\alpha_{x,i}], \tag{40}$$

$$b_{kc,i} \triangleq c_{x,i}[\gamma_{x,i}]\{\beta_{x,i}\}. \tag{41}$$

The combined system with plant, actuators, sensors, estimator, and external input shaping filters can then be realized as:

$$\{\dot{x}_{sys}\} = [A_{sys}]\{x_{sys}\} + [B_{sys}]\{\omega_x\} \tag{42}$$

where,

$$\{x_{sys}\} \triangleq \begin{Bmatrix} x_{pase} \\ x_x \end{Bmatrix}, \; [A_{sys}] \triangleq \begin{bmatrix} A_{pase} & B_{px}A_{kc} \\ 0 & A_x \end{bmatrix}, \; [B_{sys}] \triangleq \begin{bmatrix} B_{px}B_{kc} \\ B_x \end{bmatrix}, \tag{43}$$

$$[A_x] \triangleq diag[\, \alpha_{x,1} \; \alpha_{x,2} \; \ldots \; \alpha_{x,m_x} \,], \;\; [B_x] \triangleq diag[\, \beta_{x,1} \; \beta_{x,2} \; \ldots \; \beta_{x,m_x} \,], \tag{44}$$

$$[A_{kc}] \triangleq diag[\, a_{kc,1} \; a_{kc,2} \; \ldots \; a_{kc,m_x} \,], \;\; [B_{kc}] \triangleq diag[\, b_{kc,1} \; b_{kc,2} \; \ldots \; b_{kc,m_x} \,]. \tag{45}$$

$\{\omega_x\}$ is a vector of external inputs, $\omega_{x,i}(i = 1, \ldots, m_x)$, which are assumed to be ergodic uncorrelated zero mean gaussian distributed inputs with white PSD.

With a state-space realization available to model a wide class of linear system descriptions, the way this realization is used can now be discussed. To this end, the *optimization* portion of the damping allocation procedure shown in Figure 6 will now be discussed. This portion of the procedure considers each *good* candidate damper application case individually. For each case, a list of damper geometries is specified, as well as nominal viscous damping constants, and mass and stiffness properties of the dampers. The [M], [C], and [K] matrices in equation (16) are modified from their nominal values to appropriately accommodate the added dampers, and are then used to construct a modified plant model. Actuator and sensor dynamics can then be added to the plant model, a control system can

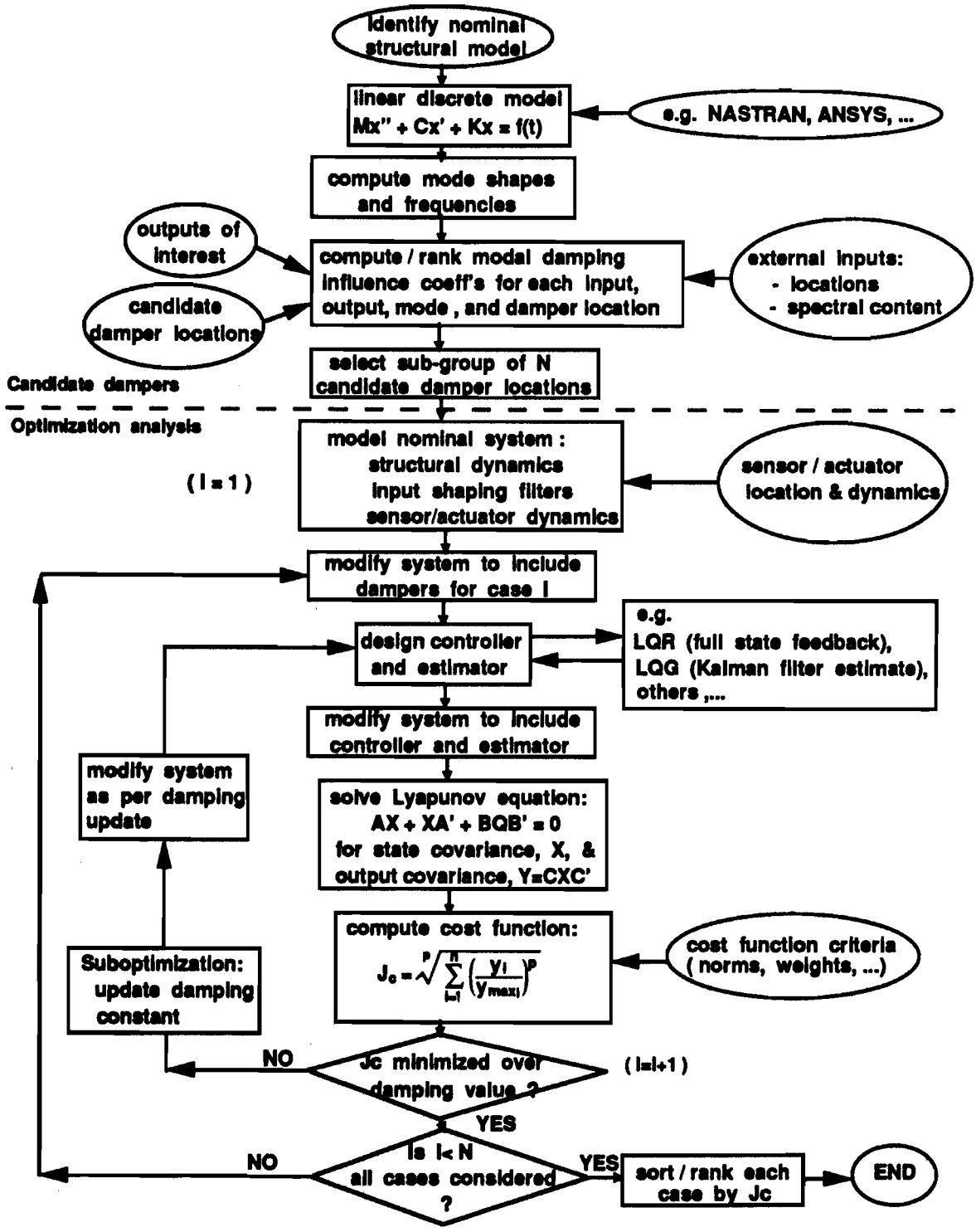

Figure 6: Damping allocation procedure flow chart

be designed as indicated in equations (32) and (33), and a system model constructed as per equation (42).

The optimal damper configuration selection is based upon minimizing a cost function constructed from RMS values of system outputs. Computing the RMS values for high order systems can be computationally intensive. For a linear system with uncorrelated inputs, one method of finding the RMS values, x_{RMS}, of a state x resulting from a random ergodic input f(t) is to perform the following integration [10]:

$$x_{RMS} = \sqrt{\frac{1}{2\pi}\int_{-\infty}^{+\infty} |G_{fx}(J\omega)|^2 \, S_f(\omega) d\omega} \quad . \tag{46}$$

$G_{fx}(J\omega)$ is the transfer function from f to x in the Laplace domain and evaluated at $s = Jw$. $S_f(\omega)$ is the PSD of f and is defined by:

$$S_f(\omega) \triangleq \int_{-\infty}^{+\infty} R_f(\tau) e^{-J\omega\tau} d\tau \tag{47}$$

where, $R_f(\tau) = E[f(t)f(t-\tau)]$ for an ergodic process. The procedure for computing and integrating $G_{fx}(J\omega)$ for all inputs and outputs is computationally intensive. A more efficient approach is to solve a continuous–time Lyapunov equation [11] of the form:

$$[A_{sys}][P] + [P][A_{sys}]^T + [B_{sys}][Q][B_{sys}]^T = 0 \tag{48}$$

for the matrix [P]. If $[A_{sys}]$ is asymptotically stable (i.e. all eigenvalues have negative real part) and [Q] is positive semidefinite, then there is a unique solution [P] which is positive semidefinite and satisfies:

$$[P] = \int_0^{\infty} e^{A_{sys}^T t} B_{sys}^T Q B_{sys} e^{A_{sys} t} dt. \tag{49}$$

If all inputs to the system are regarded as uncorrelated purely random (white PSD) inputs with unity spectral density (input shaping filters account for gain differences), then [Q] is an identity matrix and [P] is the steady–state covariance matrix for the system's states.

Now consider an m_o–vector, $\{y_o\}$, consisting of outputs of interest for the system, and related to $\{x_{sys}\}$ by:

$$\{y_o\} = [C_o]\{x_{sys}\} \tag{50}$$

The output covariance matrix, $[Y_o]$, is then given by:

$$[Y_o] = [C_o][P][C_o]^T \tag{51}$$

A vector $\{y_{RMS}\}$ of RMS outputs of interest can then be computed as the square root of the diagonal elements of $[Y_o]$.

As a computational note, equation (48) is computed in PRO–MATLAB by transforming to schur form, solving for the upper-triangular system, and then transforming back [8]. Because $[B_{sys}][B_{sys}]^T$ can be poorly conditioned, it is numerically more robust to compute

the SVD (singular value decomposition) [12,13] of $[B_{sys}]$ and then solve a related Lyapunov equation [14]. To this end, let the SVD of $[B_{sys}]$ be given by:

$$[B_{sys}] = [U][\Sigma][V^*] \text{ ,}^2 \tag{52}$$

where [U] and [V] are unitary matrices and $[\Sigma]$ is a diagonal matrix containing the singular values of $[B_{sys}]$. The following related Lyapunov equation can then be solved for $\bar{P}$:

$$[\bar{A}_{sys}][\bar{P}] + [\bar{P}][\bar{A}_{sys}]^T + [\Sigma][\Sigma]^T = 0 \tag{53}$$

where,

$$[\bar{A}_{sys}] \triangleq [U^*][A_{sys}][V] \quad \text{and} \quad [\bar{P}] \triangleq [V^*][P][U]. \tag{54}$$

The desired covariance matrix, [P], is then obtained by transforming back using $[P] = [V][\bar{P}][U^*]$.

Having obtained RMS values, the next step is to compute a cost function, J_{cost}, which is a weighted p–norm of the elements of $\{y_{RMS}\}$, and is given by:

$$J_{cost} = \left[\sum_{i=1}^{m_o} \left(\frac{y_{RMS,i}}{y_{RMS\ max,i}}\right)^p\right]^{1/p} . \tag{55}$$

The optimal damping case is that for which J_{cost} is minimized. The quantities $y_{RMS\ max,i}$ are weightings which represent the maximum tolerable values of $y_{RMS}(i = 1, \ldots, m_o)$ as determined by system level requirements. The default value used for p is 2, but any value can be used.

For each case, there is a simple sub-optimization scheme used to identify what level of damping minimizes J_{cost}. The sub-optimization scheme used modifies the nominal damping constant in each damper by the same factor. At this point the factor is chosen simplistically using a secant direct search method [15].

After addressing each case, the cases are ranked and sorted by J_{cost}.

A drawback of the optimization procedure is that it is computationally intensive both in regard to number of operations and memory requirements. Although not yet developed, it is felt that model reduction techniques can be used to handle extremely high order systems. To date, the largest system to which this optimization phase was applied contained 292 states, and required a maximum of 16 megabytes of memory. Another drawback is the current inability to easily handle the inclusion of hysteretic damping [7] either in the nominal structure, or as appended damping.

3 Candidate Damper Locations for Gravity Wave Experiment

This section provides an example of the procedure discussed in section 2.2 to identify *good* candidate damper locations. The application is the simplified finite element model

[2] [ ]* denotes Hermitian transpose of [ ]

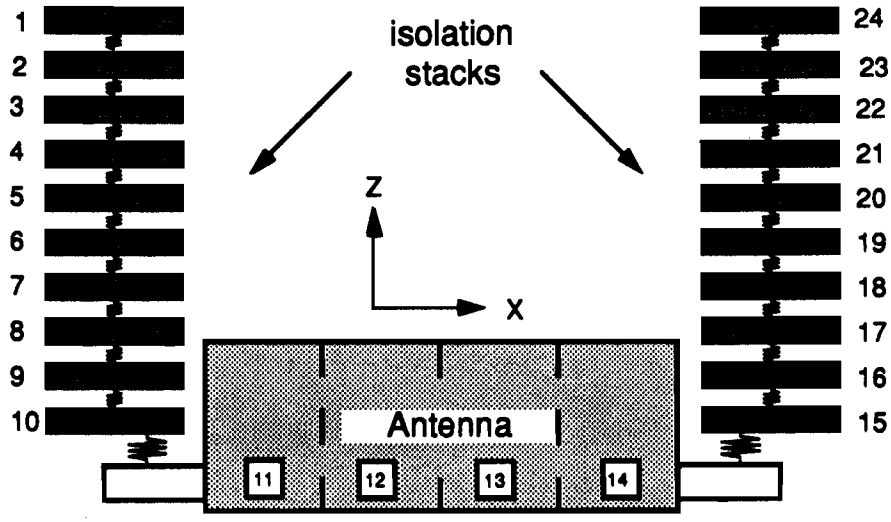

Figure 7: Simplified model of Gravity Wave Experiment structure

of the Stanford Gravity Wave experiment shown in Figure 7. The model consists of two spring–mass isolation stacks, each stack consisting of ten 6-DOF springs and masses. The isolation stacks are connected at each end of a 4 node cylindrical bar modeling the antenna. Four nodes are sufficient because primary interest is in the first longitudinal mode. The complete structure has 144 DOF.

Inputs of interest for the Gravity Wave experiment are cultural and seismic noise in the laboratory. For this example, only seismic noise is modeled, and it is assumed to be applied in three translational DOF at the top of each isolation stack. The PSD of seismic ground motion used is shown in Figure 8, and was adapted from chapter 10 of reference [16]. For the sake of this example we will regard excitation of the antenna as the sole output of interest. A measure of this excitation is the relative motion between nodes 11 and 14 in the x–direction (see Figure 7).

The objective is to place viscous dampers in the isolation stack so that they have maximal effect upon the output considered. The damper can be placed to dissipate energy due to the relative motion between any pair of masses in the isolation stack. As a result of the symmetry in this model, only one isolation stack need be considered. Using an automated PRO–MATLAB procedure, the *gain factors* of equation 13 were quickly computed for all 45 ($n(n-1)/2$, $n = 10$) possible damper locations, for all 144 modes of the model, and for the input and output specified. Among the outputs of the procedure is a 3–D contour plot of peak *gain factors* versus the damper connection coordinate pairs.

Figure 9 shows the contour plot for this case. The height of the contour at any intersection is the *gain factor* associated with placing a damper between coordinates a and b designated by the horizontal axes. A large peak and a smaller plateau stand out in the figure. The large peak indicates the effectiveness of placing dampers between coordinates 5 and 10, or between coordinates 6 and 10. The plateau indicates that dampers are effective

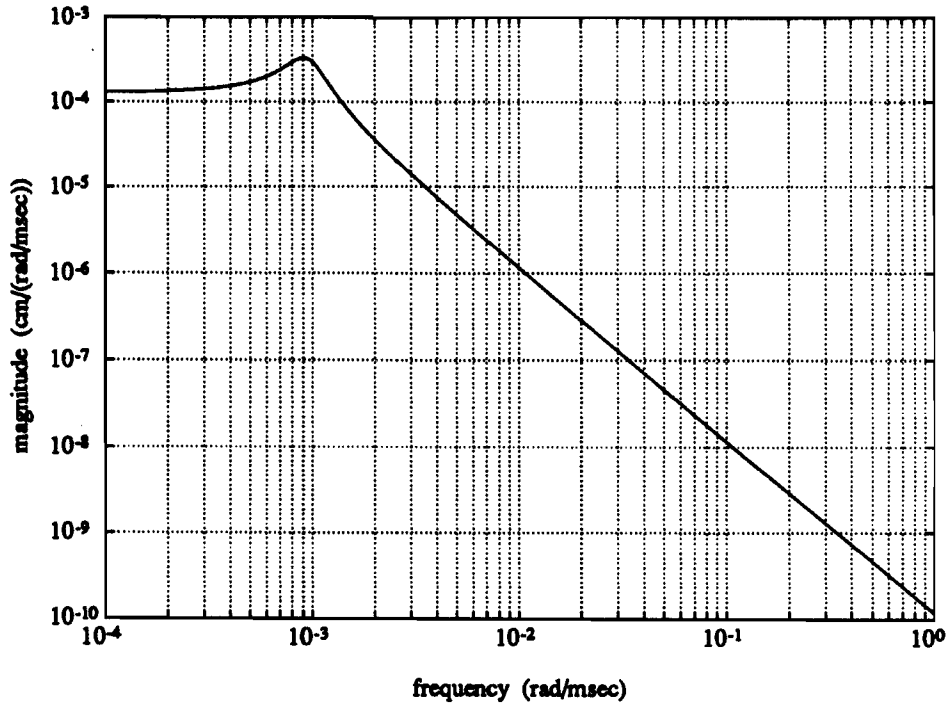

Figure 8: Position PSD coloring filter for seismic disturbances

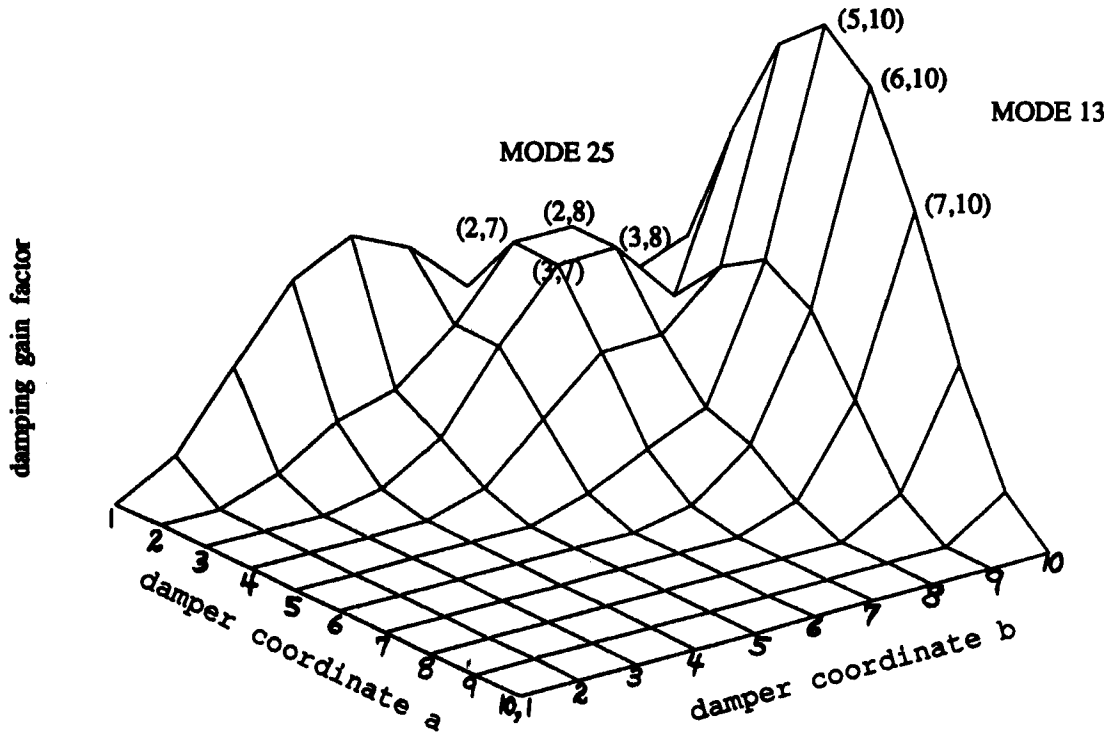

Figure 9: Contour plot of *gain factors* versus damper connection coordinate pairs for simplified Gravity Wave Experiment model

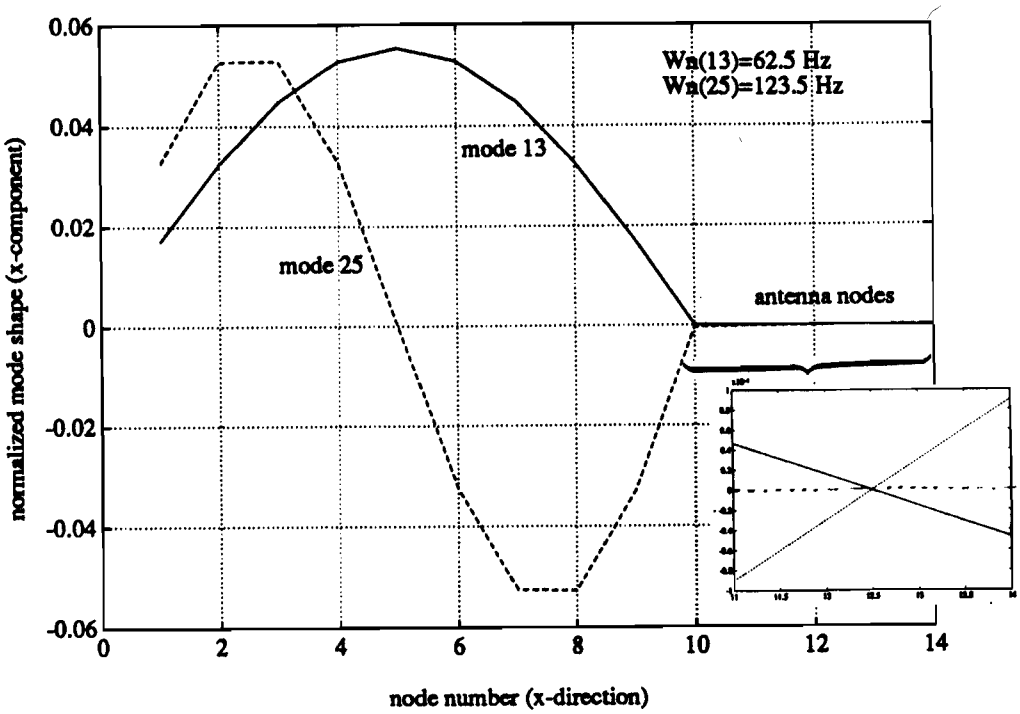

Figure 10: Normalized mode shapes for modes 13 and 25 of simplified Gravity Wave Experiment model

between coordinates coordinates 2 or 3 and coordinates 7 or 8. In addition, the program identifies the mode of vibration which produced the peak *gain factor* for a specific damper geometry. The peak in the contour is associated with the 13^{th} mode, whereas the plateau is associated with mode 25. These results are supported by the mode shape plots shown in Figure 10. Mode 13 shows substantial relative motion between coordinates 5 and 10 and between coordinates 6 and 10. Similarly, mode 25 shows large relative motion between coordinates 2 or 3 and coodinates 7 or 8. Furthermore, for both of these modes there is large relative motion between coordinates 11 and 14 (the output of interest), as indicated by the *blow-up* of coordinates 11 through 14 in Figure 10. The *blow-up* is required because the antenna is quite massive and stiff so that its motion is small relative to motion of the isolation stack elements. Another interesting result is that although mode 25 has larger relative peak-to-peak motion than mode 13, the contour plot indicates that damping mode 13 is more effective. This apparent contradiction is clarified by looking at the spectral density of the input. Figure 8 shows that for frequencies above 0.15 Hz ($\sim 9(10^{-4})$ rad/msec) the input PSD shaping filter is rolling off at 40 dB/decade. Because mode 25 is at 123.5 Hz and mode 13 is at 62.5 Hz, the input shaping filter has about 1/4 of the gain at mode 25 than at mode 13. Consequently, sufficiently more disturbance energy density at the frequency of mode 13 makes this mode the more desirable mode to damp.

Note that the above example was provided primarily to illustrate the procedure that generates *good* candidate damper locations. For application to the actual Gravity Wave Experiment, a more detailed finite element model of the system was used, and the outputs of interest identified in section 1.2 were considered.

4 Optimal Allocation for Gravity Wave Experiment

This section discusses the application of the optimization procedure described in section 2.3 to a collection of candidate damper configurations generated as discussed in section 3. Because there is no active control for this example, the nominal system need only be modified to include appended dampers and the external disturbance filter states. As in section 3, the inputs are comprised only of seismic disturbances acting in 3 DOF at the top of each isolation stack. The appended dampers were assumed to have negligible stiffness and mass, an assumption which can be abandoned in future studies as the damping hardware becomes defined better.

The outputs to be optimized for this case provide an interesting sample application of the procedure. The optimization objectives are summarized as follows:

- Minimize the RMS dynamic strain in all of the isolation springs.
- Minimize the average rate of energy dissipation as heat.
- Maximize the amount of isolation provided to the antenna at the antenna's longitudinal resonance frequency.
- Maximize the Q in the antenna longitudinal mode (i. e. do not damp the antenna mode).

RMS dynamic strains in the translation degrees of freedom of each spring are computed as the RMS dynamic stretch in each spring divided by the static vertical deflection in each spring. Average power dissipation as heat is computed for each damper as the damping constant times the covariance of the relative velocity between the damper connection coordinates. RMS motion between the antenna end faces is used as an approximate measure of the isolation of the antenna longitudinal mode. Since no appropriate measure of the Q in the antenna's longitudinal mode is available from the RMS state outputs, this figure of merit was excluded from the optimization. Verification that the inherent Q in the antenna's longitudinal mode was not significantly reduced by the added damping was performed after the optimization by studying the resulting frequency responses.

The cost function, J_{cost}, constructed for this application is given below:

$$J_{cost} = \sqrt{\left(\frac{\epsilon_{max}}{\epsilon_{max_{allow}}}\right)^2 + \left(\frac{\dot{E}_{heat}}{\dot{E}_{heat_{allow}}}\right)^2 - \left(\frac{antenna_{excite}}{antenna_{excite_{allow}}}\right)^2}. \tag{56}$$

ϵ_{max} is the maximum RMS strain in all springs of the isolation system with all degrees of freedom considered. $\dot{E}_{heat}$ is the total rate of energy dissipation as heat in all dampers for each case considered. $antenna_{excite}$ is the RMS relative motion between the antenna's end faces. The weighting factors designated by the notation $(\ )_{allow}$ represent the maximum allowable values of the quantites in $(\ )$ as determined by system level requirements. These requirements are listed in Table 2.

The structure of this optimization provides for interesting trade-offs. First of all, the allocation of damping must be such that it damps all isolation modes with a minimal

Quantity	Requirement	Current value
max. RMS dynamic stress in isolation	< 1% of 0.2% spring spring yield stress	~0.2% of 0.2% spring yield stress
max. average heat dissipation in dampers	< 10 μW in 40 mK region	~0.18 μW per damper * 8 = 1.44 μW
antenna isolation	~ 300 dB	~250 dB
antenna resonance Q	$\approx 10^7$	$\approx 10^7$

Damping required in 6 DOF :

direction	x, y, z (N-s/m)	θ_x, θ_y (N-s-m)	θ_z (N-s-m)
damping constant	300	0.1	0.2

Table 2: Baseline design requirements for added damping in Gravity Wave Experiment

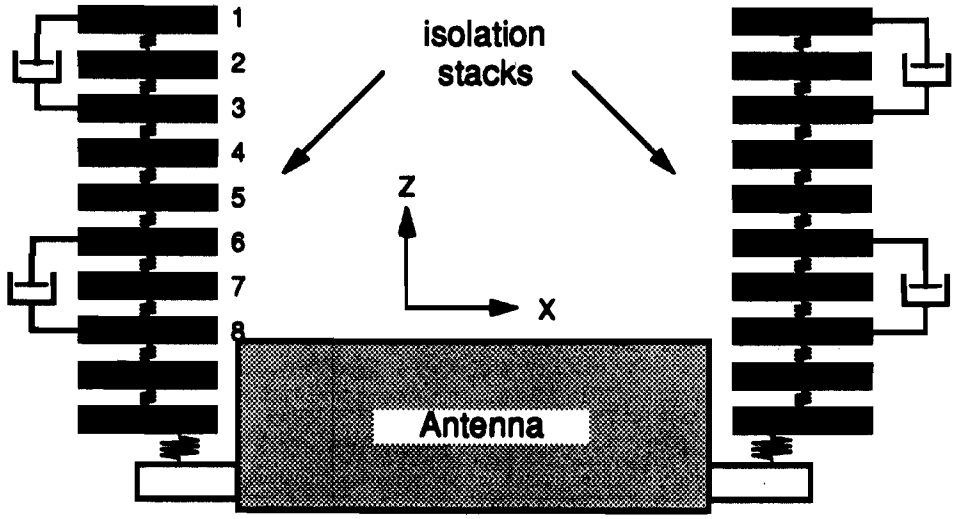

Figure 11: Baseline damping allocation for simplified model of Gravity Wave Experiment structure

number of dampers, and yet does not damp the antenna mode or compromise the isolation. Secondly, the desire to minimize RMS dynamic strains tends to demand large damping constants, whereas the requirements to minimize heat dissipation and maximize antenna isolation at the antenna resonance tend to reduce the desired damping constants.

5 Baseline Damping Allocation and Design Requirements

Application of the optimization procedure produced a set of baseline damping allocation requirements. The procedure was used to identify the effectiveness of using either one or two 6-DOF dampers for each isolation stack. Using two dampers per stack provided enough performance improvement, as measured by the cost function J_{cost}, to warrant the additional hardware. The baseline allocation is shown in Figure 11. Applying 6-DOF of damping between the 1^{st} and 3^{rd} stages, and between the 6^{th} and 8^{th} stages of each isolation stack was considered optimum by the procedure.

Note, that the locations identified in section 3 are quite different from the *optimum* locations obtained. One reason for this apparent discrepancy is that the criteria of antenna excitation used in section 3 was just one of three criteria used in the optimization of section 4 (see equation 56). Secondly, antenna excitation is a quantity to be *minimized* since it is used as a measure of the isolation provided to the antenna.

Table 2 compares system requirements with values obtained from the optimization procedure for the quantities specified in section 4. As discussed in section 1.2, the requirement on maximum RMS dynamic strain in the isolation springs is intended to minimize the probability of nonlinear *creaking* in the isolation system. The design value of 0.2% of

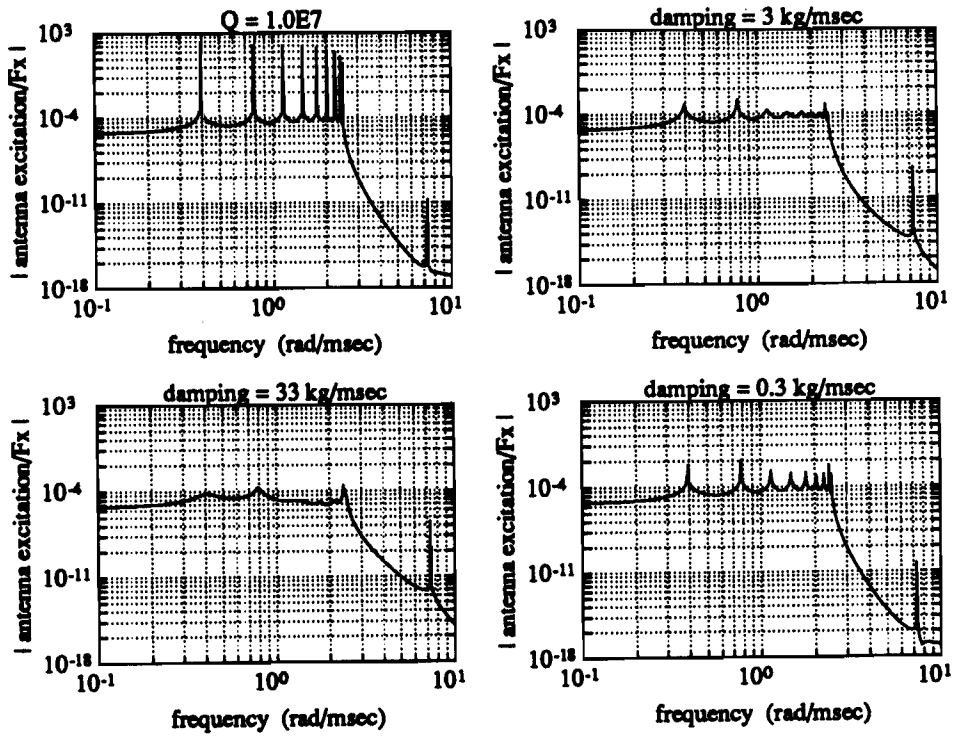

Figure 12: Frequency responses from input at top of isolation stack in x-direction to antenna excitation with added damping in baseline configuration and damping constants of: (a) 0, (b) 3 kg/msec, (c) 33 kg/msec, and (d) 0.3 kg/msec

the 0.2% yield stress is well within the 1% maximum. Assuming that the entire isolation system is enclosed in the 40 mK region, the maximum tolerable heat dissipation is 10 μW. For the baseline design there is an energy dissipation rate as heat of about 0.18 μW per damper, or about 1.44 μW for all eight dampers, which is well within the requirement.

Note that the current isolation system design does not meet the isolation requirement. This condition, however, is primarily associated with the stiffness of the springs modeled. Figure 12 shows the frequency responses from a disturbance excitation at the top of the isolation stacks in the x-direction (see Figure 11) to relative motion between the antenna end faces for various damping constant values. As can be seen from Figure 12(a), even with no added damping, the isolation provided to the antenna at the antenna resonance is about 250 dB. The springs currently being designed, and which will be used for future modeling, will be made less stiff to improve the isolation. It remains to be seen to what extent the reduced stiffness impacts the ability to meet the dynamic strain requirements.

As can also be seen in Figure 12, the level of damping used at the baseline damper locations has an interesting impact upon the isolation to the antenna mode, and upon the Q of the resonant peaks in the isolation modes. Figure 12(b) shows that for a damping constant of 3 kg/msec in all translational dampers, the resonant Q's of the isolation system are substantially reduced from 10^7 to about $10^1 - 10^2$, but the isolation to the antenna mode is reduced by 45 dB. As the damping is increased to 33 kg/msec, the isolation system's maximum resonant Q's are reduced further to about 10^1, but the isolation to the antenna is reduced by about 80 dB. Figure 12(d) shows the frequency response for the design

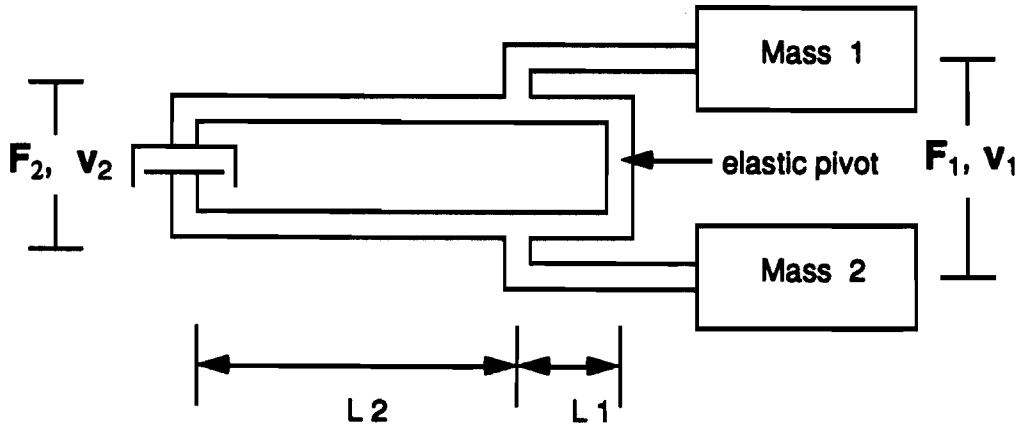

Figure 13: *Concept* for matching impedances between stiffness and damping elements

damping values given in Table 2, and indicates that the maximum isolation resonant Q's are reduce to less than 10^3, while the isolation to the antenna mode is reduced by only 24 dB. The design damping constant values provide a good compromise between resonant peak reduction in the modes of the isolation system, and the level of isolation provided to the antenna at the antenna longitudinal resonance. Note that the damping allocation is such that for all damping constant values used in Figure 12, the resonance Q of the antenna's 1^{st} longitudinal mode deviates indistinguishably from its undamped value of 10^7.

6 Damping–Stiffness Impedance Matching

Section 1.2 discussed issues associated with realizing damping in the Stanford Gravity Wave Experiment. This section discusses still another important damping realization issue, namely the impedance mismatch between the stiffness acting between the isolation system's masses (see section 1.1) and the damping to be used between the masses. A feature of the optimization procedure discussed in section 2.3 is the computation of RMS values for all states of the system. For the model of seismic motion used, typical RMS dynamic forces are about $0.15 - 0.5$ N. Recall that these forces are associated with the stretching of the isolation springs. Typical RMS dynamic torques are about $2(10^{-3})$ N-m. RMS relative velocities between masses of the isolation system are about 1 μm/sec. From the standpoint of damping implementation, these quantities represent an impedance mismatch. A viscous damper which provides a comparable level of force for these velocities would require a damping constant of about $3(10^5)$ N-sec/m. This would require the construction of a sizable damping element.

This impedance mismatch can be reduced, however. The idea, illustrated purely conceptually in Figure 13, is to use a lever mechanism to amplify the motion of interest. Consider an RMS force F_1 acting between masses 1 and 2 in the figure, and an associated RMS relative velocity v_1. By using the advantage shown, the relative velocity can be am-

plified at a remote location by the leverage ratio L_2/L_1, where L_1 and L_2 are as shown ($L_1 < L_2$). Consequently the magnified velocity is $v_2 = \left(\frac{L_2}{L_1}\right) v_1$. In addition, the remote force F_2 which would cause the same motion between masses 1 and 2 as F_1 is related to F_1 by $F_2 = \left(\frac{L_1}{L_2}\right) F_1$. A damper sized to match the stiffness impedance at location (1) is given by $b_1 = F_1/v_1$, and the rate of energy dissipation resulting from this damper is given by $\dot{E}_1 = b_1 v_1^2$.

A damper sized to match the stiffness impedance at location (2) is given by:

$$b_2 = \frac{F_2}{v_2} = \left(\frac{L_1}{L_2}\right)^2 \frac{F_1}{v_1} = \left(\frac{L_1}{L_2}\right)^2 b_1 \tag{57}$$

and the energy dissipation rate for this damper is:

$$\dot{E}_2 = b_2 v_2^2 = \left(\frac{L_1}{L_2}\right)^2 b_1 \left(\frac{L_2}{L_1}\right)^2 v_1^2 = b_1 v_1^2 = \dot{E}_1 \tag{58}$$

Consequently, if $L_1 << L_2$, then equations (57) and (58) indicate that the same energy dissipation rate can be obtained at (2) as at (1) by using a damper with a factor of $(L_1/L_2)^2 << 1$ less damping constant than used at (1).

This impedance matching concept is key to constructing reasonably sized damping elements for application to the Stanford Gravity Wave Experiment. Furthermore, because of the experiment's sensitivity to nonlinear components, it is important that the mechanism used for motion amplification have no *sloppy* joints. Hinging elements based solely upon the elastic deformation of materials, such as the concept shown in Figure 13, are consequently an important requirement.

7 Status / Conclusions

This paper has motivated and discussed the need for damping in the high order, cryogenically maintained, and nominally extremely lightly damped isolation system of the Stanford Gravity Wave Experiment. Issues associated with realizing damping in this system were mentioned and the selection of passive magnetically induced eddy-current damping as a baseline was discussed.

A general procedure aimed at optimally allocating and sizing viscous damping in controlled flexible structures was introduced. Characteristics of the procedure were motivated, underlying assumptions were discussed, and algorithmic details were developed. This design procedure was applied to the Stanford Gravity Wave Experiment system using a unique set of optimization criteria. The result was the specification of reasonable baseline damping allocation design requirements which provide a good compromise between the various optimization objectives.

The eddy-current dampers to be used for 6–DOF of damping in the Gravity Wave Experiment are currently being designed. The importance of a damping–stiffness structural impedance match was mentioned, and mechanisms for providing this match are being worked into the damper design process. Work is also in progress to refine the stiffness values used in modeling the system.

References

[1] P. F. Michelson, W. M. Fairbank, J. Henderson, K. Lane, M. S. McAshan, J. C. Price, T. Stevenson, R. C. Taber, and B. Vaughan. The Stanford Gravitational Wave Detection Program: A Plan for Observing the Next Supernova. In *International Symposium on Experimental Gravitational Physics*, August 1987.

[2] Peter F. Michelson, John C. Price, and Robert C. Taber. Resonant-Mass Detectors of Gravitational Radiation. *Science*, 237:150–157, July 1987.

[3] John C. Price. Optimal Design of Resonant–Mass Gravitational Wave Antennas. *Physical Review D, Particles and Fields*, 36(12):3555–3570, December 1987.

[4] V. B. Braginsky, V. P. Mitrofanov, and V. I. Panov. *Systems with Small Dissipation.* The University of Chicago Press, 1985.

[5] Peter Veitch. *Development and Preliminary Operation of a Cryogenic Gravitational Radiation Antenna.* PhD thesis, University of Western Australia, 1986.

[6] F. J. Laner, editor. *Acoustic Emission.* IFI/Plenum, New York, 1979.

[7] Ahid D. Nashif, David I. G. Jones, and John P. Henderson. *Vibration Damping.* John Wiley and Sons, 1985.

[8] Cleve Moler, John Little, and Steve Bangert. *PRO-MATLAB^{TM} User's Guide.* The MathWorks, Inc., 21 Eliot Street, South Natick, MA, August 1988.

[9] Arthur E. Bryson, Jr. and Yu-Chi Ho. *Applied Optimal Control.* Hemisphere Publishing Corporation, Washington, D.C., 1975.

[10] Leonard Meirovitch. *Analytical Methods in Vibrations.* Macmillan Publishing Co., Inc., New York, N.Y., 1967.

[11] H. Kwakernaak and R. Sivan. *Linear Optimal Control Systems.* Wiley-Interscience, New York, 1972.

[12] Ben Noble. *Applied Linear Algebra.* Prentice-Hall, Inc., Englewood Cliffs, New Jersey, 1969.

[13] C. B. Moler and G. E. Forsythe. *Computer Solution of Linear Algebraic Systems.* Prentice-Hall, Inc., Englewood Cliffs, New Jersey, 1967.

[14] A. Laub. Computation of Balancing Transformations. In *JACC*, 1980.

[15] P. E. Gill, W. Murray, and M. H. Wright. *Practical Optimization.* Academic Press, Inc., London, England, 1981.

[16] K. Aki and P. Richards, editors. *Quantitative Seismology : Theory and Methods.* Volume 1, Freeman and Co., 1980.